Two-dimensional hole gas and Fermi-edge singularity in Be δ-doped GaAs

D. Richards,* J. Wagner, H. Schneider, G. Hendorfer,† and M. Maier
Fraunhofer-Institut für Angewandte Festkörperphysik, Tullastrasse 72, D-7800 Freiburg, Federal Republic of Germany

A. Fischer and K. Ploog‡
Max-Planck-Institut für Festkörperforschung, Heisenbergstrasse 1, D-7000 Stuttgart 80, Federal Republic of Germany
(Received 15 April 1992; revised manuscript received 24 November 1992)

The subband structure of the quasi-two-dimensional hole gas (2DHG) formed at a single Be δ-doped layer in GaAs has been studied by photoluminescence spectroscopy. To confine the photogenerated minority carriers, and thus to enhance the efficiency of radiative recombination from the 2DHG, the δ-doping spike was placed in the center of an $Al_xGa_{1-x}As/GaAs/Al_xGa_{1-x}As$ double heterostructure. Recombination involving different hole subbands has been resolved which enabled us to analyze the subband occupation as a function of dopant concentration and sample temperature. In sample structures where the Fermi level is located close to unoccupied subbands, a pronounced Fermi-edge singularity (FES) is observed in the low-temperature (<20 K) luminescence spectrum. The temporal evolution of the FES has been studied by time-resolved luminescence spectroscopy. The enhancement in emission intensity at the Fermi edge can be understood in terms of a transfer of excitonic oscillator strength from the unoccupied subbands to nearby occupied states at the Fermi energy. Self-consistent subband calculations have been performed to compute the hole confining potential and the subband energies for the present δ-doped structures. The results of these calculations, which take into account the finite spread of the dopant atoms in accordance with secondary-ion-mass spectroscopic data, are in good agreement with the measured subband spacings. The assignment of light- and heavy-hole transitions is supported by luminescence measurements using circularly polarized light.

I. INTRODUCTION

There is considerable current interest in so-called δ (or planar) doping of semiconductors. This is because of the possibility of fundamental studies based on δ-doped structures as well as a variety of promising applications in semiconductor devices.[1] An isolated doping spike of, e.g., Si or Be in GaAs forms a two-dimensional electronic system. The electrons or holes are confined in a space-charge-induced potential well leading to a two-dimensional electron gas (2DEG) or hole gas (2DHG) where usually several subbands are occupied.[1,2] So far most of the studies have been carried out on *n*-type Si δ-doped GaAs layers. Both the incorporation and the depth distribution of the dopant atoms[3–9] as well as the structure and population of the electron subbands[2,3,6,10–12] have been investigated with a variety of experimental techniques. Also self-consistent subband calculations have been performed by a number of groups and used, e.g., to deduce the actual width of the Si doping spike from experimental data on the occupation of the various subbands.[3,5,6,10–13] Only recently has *p*-type δ doping of GaAs been investigated in some detail.[14–17] These investigations include secondary-ion-mass spectroscopy (SIMS),[15] capacitance profiling,[15] and direct imaging by high-resolution transmission electron microscopy[6] to assess the spatial distribution of the dopant atoms. Photoluminescence (PL) measurements on Be δ-doped GaAs layers have been used to gain information on the subband structure and occupation.[17] Still lacking are self-consistent subband calculations for *p*-type δ-doped GaAs structures which would allow a direct comparison with experimental data.

In δ-doped layers PL spectroscopy is complicated by the fact that the potential confining the majority carriers is repulsive for the photogenerated minority carriers. In *n*-type δ-doped GaAs layers this repulsive interaction leads to a too large spatial separation of the carriers to observe efficient radiative recombination from the 2DEG.[18,19] It has been shown that confining the minority carriers by $GaAs/Al_xGa_{1-x}As$ heterointerfaces placed sufficiently close to the δ-doping layer enhances the wave-function overlap such that efficient emission from the 2DEG can be observed.[20,21] For *p*-type δ-doped layers the repulsion of the minority carriers by the hole confining potential seems to have less effect on the luminescence efficiency because radiative recombination from the 2DHG has been reported from plain Be δ-doped GaAs layers.[22] But also there, as will be shown below, placing the Be doping spike in the center of an $Al_xGa_{1-x}As/GaAs{:}Be/Al_xGa_{1-x}As$ double heterostructure leads to a significant enhancement of the 2DHG emission intensity.[17]

Fermi-edge singularities (FES) have been studied in detail in *n*-type modulation-doped heterojunctions and quantum wells.[23–31] The FES, which manifests itself by an enhancement of the luminescence intensity at the Fermi edge, is a consequence of many-body interactions between electrons and holes.[24,32–35] To observe this effect in the emission spectrum either non-*k*-conserving transitions have to contribute to the luminescence spectrum[23,27] or the excitonic oscillator strength of unoccu-

pied subbands at energies close to the Fermi level has to be transferred to occupied states at the Fermi edge.[33,34] In a 2DHG system Fermi-edge singularities have been observed only recently in the luminescence spectrum of a dense 2DHG in a δ-doped $Al_xGa_{1-x}As/GaAs:Be/Al_xGa_{1-x}As$ structure.[17]

In the present paper a detailed PL study of Be δ-doped GaAs layers will be presented including time-resolved PL measurements and experiments with circularly polarized light. To assign the various emission bands observed in PL to transitions involving specific hole subbands, self-consistent subband calculations have been performed. The results of these calculations compare favorably well with measured subband spacings. For this comparison the energetic position of the Fermi level can readily be extracted from the PL spectra because a pronounced FES is observed in samples where the Fermi level lies close to unoccupied subbands.

The organization of this paper is as follows. In Sec. II details of the samples and of the photoluminescence experiments are described. The experimental luminescence data are presented in Sec. III. In Sec. IV numerical results of the self-consistent subband calculations are discussed and compared to the experimental data. The conclusions are given in Sec. V.

II. EXPERIMENT

The samples used for the present study were grown by molecular-beam epitaxy on undoped semi-insulating (100) GaAs substrates at substrate temperatures of 580 °C (samples nos. 1–3) or 610 °C (sample no. 4), respectively. Sample no. 1 consists of a thick GaAs layer with a Be δ-doping spike placed at a nominal depth of 20 nm underneath the surface. The intended doping level was 8×10^{12} cm^{-2}. For samples nos. 2–4, after a thick GaAs buffer layer or a GaAs/AlAs superlattice buffer a 20-nm-thick $Al_{0.33}Ga_{0.67}As$ barrier was grown followed by a 60-nm-wide GaAs layer. In the middle of this layer, growth was interrupted to deposit the Be doping spike with a doping concentration of 3×10^{12} cm^{-2} (sample no. 2), 8×10^{12} cm^{-2} (no. 3), and 3×10^{13} cm^{-2} (no. 4). On top of the δ-doped GaAs layer another 10-nm-thick $Al_{0.33}Ga_{0.67}As$ barrier was grown followed by a 1–2-nm-thick GaAs capping layer. The actual dopant concentrations and widths of the doping spikes were measured by secondary-ion-mass spectroscopy for samples nos. 2–4. For the lowest doping level of 3×10^{12} cm^{-2} a Be SIMS depth profile with a full width at half maximum (FWHM) of 6.5 nm was obtained. This width corresponds essentially to that of the SIMS depth resolution profile for the present experimental conditions (3.2 keV, normal incidence O_2^+ primary ions). For the highest dopant concentration of 3×10^{13} cm^{-2} (sample no. 4) a spike width of 12.5 nm was found which indicates the onset of a segregation- and/or diffusion-induced broadening for this doping level and substrate temperature.[15] The SIMS data for the different samples are listed in Table I together with the free-hole concentrations determined from Hall-effect measurements. For a dopant level of $\geq 8\times10^{12}$ cm^{-2} there is a reasonable agreement between the SIMS and the Hall concentration considering the respective experimental accuracies of ±10%. In particular, the Hall-effect measurements may not give the true hole concentrations due to the differing mobilities of the various occupied subbands.[10] For the lowest dopant concentration the free-hole concentration is significantly lower than the Be concentration, most probably due to surface depletion effects. A schematic energy-band diagram of the *p*-type δ-doped $Al_{0.33}Ga_{0.67}As/GaAs/Al_{0.33}Ga_{0.67}As$ double heterostructures (samples nos. 2–4) is shown in Fig. 1.

TABLE I. Free-hole concentrations p_{Hall} measured by Hall-effect and Be concentrations $[Be]_{SIMS}$ measured by SIMS for the δ-doped samples used in the present study. The accuracy of the Hall-effect and SIMS data is ±10%. Also given is the full width at half maximum of the Be doping spike as measured by SIMS.

Sample no.	p_{Hall} (cm^{-2})	$[Be]_{SIMS}$ (cm^{-2})	FWHM (nm)
1	a	8×10^{12} [b]	a
2	7.4×10^{11}	3×10^{12}	6.5
3	9.2×10^{12}	8×10^{12}	7.2
4	3.1×10^{13}	3×10^{13}	12.5

[a]Not measured.
[b]Nominal.

The cw PL spectra were excited with various lines of a Kr-ion laser or with the tunable output of a Ti-sapphire laser pumped by an Ar-ion laser. The samples were cooled by He exchange gas in a continuous-flow variable-temperature cryostat. The emitted light was dispersed in a single or double monochromator and detected by a cooled intrinsic Ge diode. For time-resolved measurements optical excitation was provided by a mode-locked Ti-sapphire laser producing 1-ps pulses

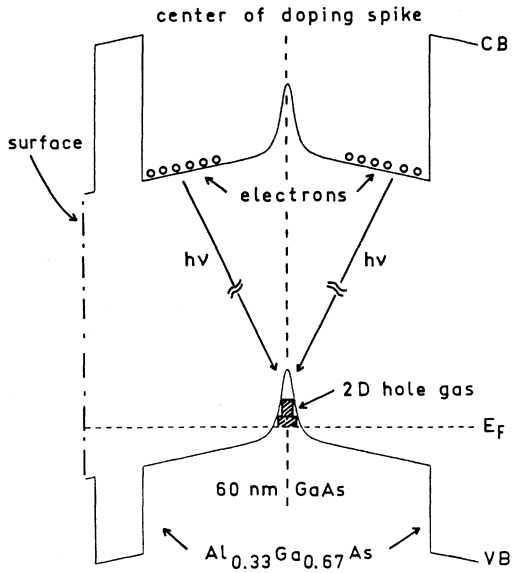

FIG. 1. Schematic energy-band diagram of the Be δ-doped $Al_xGa_{1-x}As/GaAs/Al_xGa_{1-x}As$ double heterostructure used in the present study.

at a repetition rate of 76 MHz. For excitation with photon energies well above the GaAs band-gap energy the output of the mode-locked Ti-sapphire laser was frequency doubled. On the detection side a synchroscan streak camera coupled to a single monochromator was used. The overall time resolution of the system was ≤ 50 ps.

III. PHOTOLUMINESCENCE RESULTS

Figure 2 shows low-temperature (6 K) luminescence spectra of sample no. 1 which contains no $Al_xGa_{1-x}As$ barriers. The spectra were excited at 3.00 eV to minimize the depth of the optical excitation $1/\alpha$ to 20 nm,[36] which is the nominal depth of the Be doping spike in that sample. Here α denotes the absorption coefficient. The spectra are dominated by bound exciton recombination (BE) at 1.514 eV from the undoped GaAs buffer layer. Emission from the 2DHG induced by the Be δ-doping spike is resolved as a broad band centered at 1.475 eV. With decreasing excitation intensity the relative intensity of the 2DHG emission decreases and band-to-acceptor (eA) emission from the buffer layer can be resolved at 1.493 eV. Spectral position and shape of the present 2DHG emission band are very similar to those reported in Ref. 22 for Be δ-doping spikes placed 0.5 μm underneath the surface.

A similar sequence of PL spectra is displayed in Fig. 3 for sample no. 3 where the doping spike with the same Be concentration is positioned in the center of a 60-nm-wide GaAs layer sandwiched between two $Al_xGa_{1-x}As$ barriers. Under identical experimental conditions the intensity of the 2DHG emission is enhanced by a factor of 50 and no bound exciton luminescence is observed from the GaAs buffer layer. On the top of the 2DHG emission band a peak is resolved at 1.490 eV which sharpens with increasing excitation intensity. Based on its temperature dependence this feature can be assigned to a Fermi-edge enhancement of the emission intensity (see below). The shoulder on the high-energy side of the 2DHG emission band, which is most pronounced for low excitation intensities, is most likely due to eA recombination from the GaAs buffer layer.

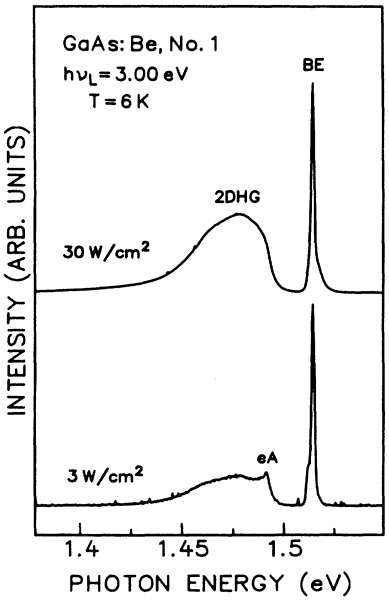

FIG. 2. Excitation-intensity-dependent photoluminescence spectra of Be δ-doped GaAs (sample no. 1). The spectra excited at 3.00 eV were recorded with the sample cooled to 6 K.

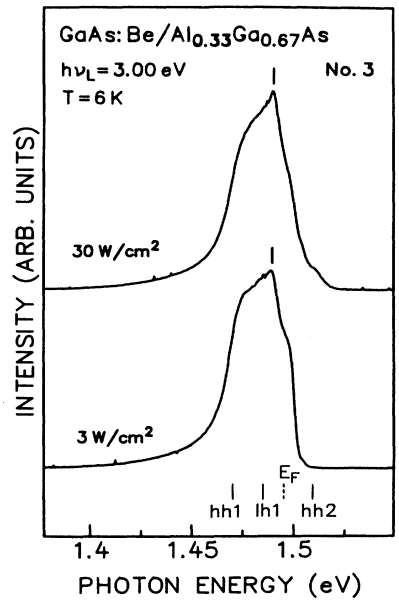

FIG. 3. Same as Fig. 2 for a δ-doped $Al_{0.33}Ga_{0.67}As/GaAs:Be/Al_{0.33}G_{0.67}As$ double heterostructure (sample no. 3). The emission intensity is $\simeq 50$ times that from the 2DHG of sample no. 1 (see Fig. 2). Calculated $k_{\parallel}=0$ subband energies are marked at the bottom of the figure (see Sec. IV). Calculations are for an 8×10^{12} cm^{-2} Be density and a dopant spread $\Delta z=2$ nm. Heavy- and light-hole character are denoted by "hh" and "lh," respectively. "E_F" marks the Fermi energy.

Comparing Figs. 2 and 3 it is evident that the insertion of the $Al_xGa_{1-x}As$ barriers significantly improves the luminescence properties of *p*-type δ-doped GaAs layers. Therefore we shall focus in the following on the sample structures with $Al_xGa_{1-x}As$ barriers (samples nos. 2–4). Figure 4 displays the low-temperature (6 K) PL spectra of those samples all recorded with excitation at 3.00 eV. When the Be concentration is increased from 3×10^{12} cm^{-2} (sample no. 1) to 8×10^{12} cm^{-2} (sample no. 3) the 2DHG emission band increases in width and shifts slightly to lower energies. A further increase of the Be concentration to 3×10^{13} cm^{-2} (sample no. 4) results in a splitting of the 2DHG emission into two bands, one centered at 1.460 eV and the other at 1.496 eV. The low-energy edge of the 1.460-eV band is shifted to even lower energies as compared to sample no. 3. On the high-energy side of the 1.496-eV emission a distinct peak is resolved. Based on its temperature dependence, i.e., its disappearance for temperatures >20 K,[17] this enhancement in intensity for transitions from states close to the Fermi level has been identified as a Fermi-edge singularity. Similar features, even though less pronounced, are resolved also

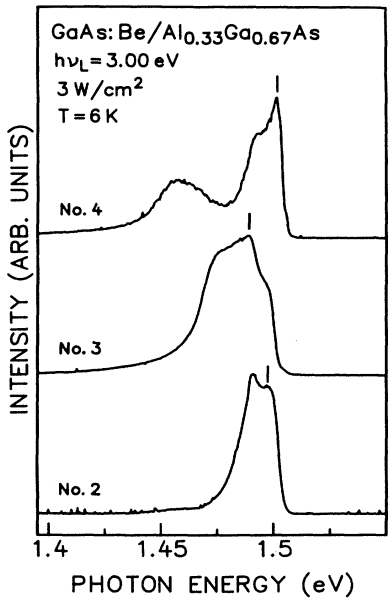

FIG. 4. Low-temperature (6 K) photoluminescence spectra of δ-doped $Al_{0.33}Ga_{0.67}As/GaAs:Be/Al_{0.33}Ga_{0.67}As$ double heterostructures with varying dopant concentration (samples no. 2–4). The vertical lines mark the enhancement in luminescence intensity at the Fermi edge.

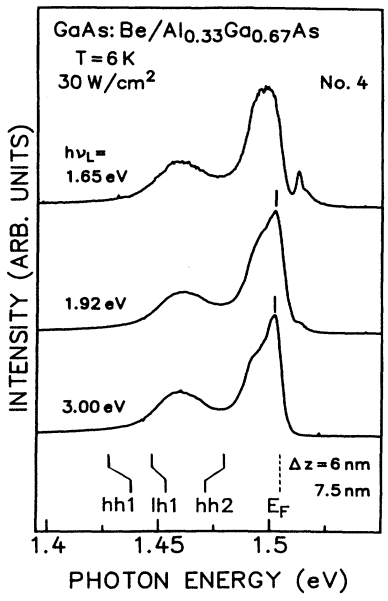

FIG. 5. Low-temperature (6 K) photoluminescence spectra of a δ-doped $Al_{0.33}Ga_{0.67}As/GaAs:Be/Al_{0.33}Ga_{0.67}As$ double heterostructure (sample no. 4) excited at different photon energies given in the figure. The vertical lines mark the enhancement in luminescence intensity at the Fermi edge. Calculated $k_{\parallel}=0$ subband energies are marked at the bottom of the figure (see Sec. IV). The calculations are for 3×10^{13} cm^{-2} acceptors and varying dopant spread Δz. Heavy- and light-hole character are denoted by "hh" and "lh," respectively. "E_F" marks the Fermi energy.

in the two less heavily doped samples nos. 2 and 3. The photoluminescence excitation (PLE) spectrum of the 2DHG emission, with an absorption cutoff at 1.515 eV in all three samples, was found to reflect the intrinsic absorption spectrum of the GaAs layer to the left and to the right of the Be δ-doping spike.

Figure 5 displays a series of PL spectra from the most heavily doped sample no. 4 excited at different photon energies. The FES is most pronounced for excitation at 3.00 eV, still resolved for 1.92-eV excitation, but completely missing for excitation at 1.65 eV which is below the band-gap energy of the $Al_{0.33}Ga_{0.67}As$ barriers. The emission peak observed at 1.513 eV in the topmost spectrum in Fig. 5 is due to bound exciton luminescence from the buffer layer. It is interesting to note that the FES is only observed for excitation above the barrier band-gap energy. It is particularly well resolved for excitation with 3.00-eV photons which are absorbed within the first 20–30 nm underneath the surface. This might be related to the fact that such excitation generates electron-hole pairs only on the near-surface side of the doping spike which in principle changes the electrostatic potential in an asymmetric way. This change in potential shape may modify the overlap between electron and hole wave functions, possibly favoring the observation of a FES in the PL spectrum.

Time-resolved PL spectra of sample no. 4 are plotted in Figs. 6 and 7 for excitation at 1.73 and 3.07 eV, respectively. The overall shape of the time-resolved PL spectra resembles very much that of the cw spectra excited at the corresponding photon energies (see Fig. 5). For excitation at 1.73 eV (Fig. 6) the main peak in the time-resolved PL spectra shows a slight redshift and a reduction in

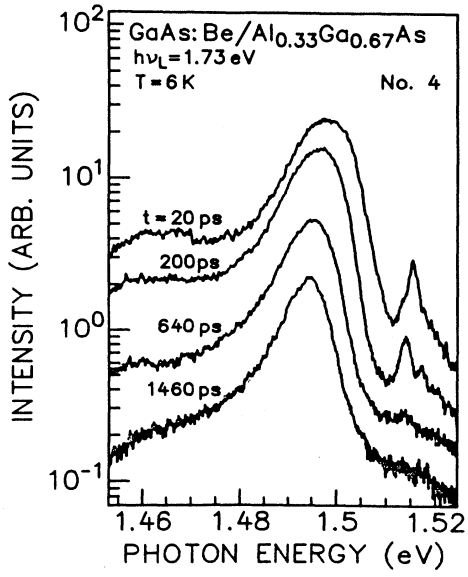

FIG. 6. Time-resolved photoluminescence spectra of sample no. 4 excited at 1.73 eV.

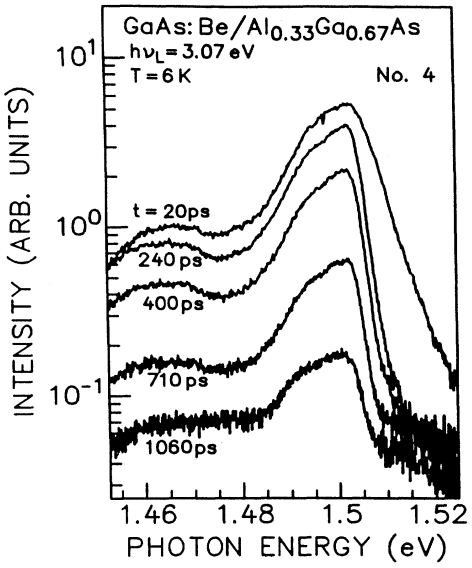

FIG. 7. Same as Fig. 6 for excitation at 3.07 eV.

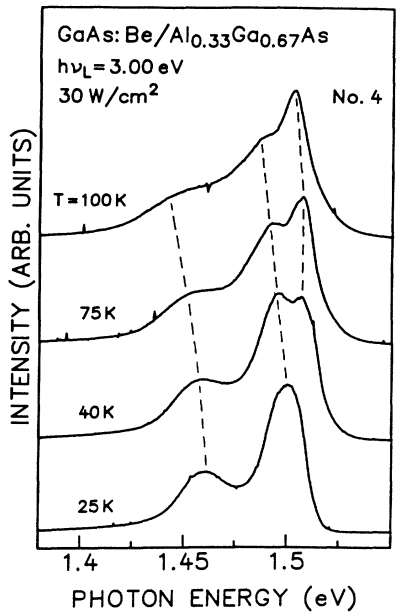

FIG. 8. Temperature-dependent photoluminescence spectra of sample no. 4 excited at 3.00 eV.

peak width with increasing delay time t after the exciting laser pulse. This trend reproduces that observed in cw luminescence spectra upon reduction of the excitation intensity. There the corresponding PL peak narrows and shifts to lower energies when the excitation intensity is reduced (see Fig. 2 in Ref. 17). This similarity suggests that the changes in the time-resolved PL spectra with increasing delay time are essentially due to the decreasing number of photogenerated carriers as they gradually recombine. Emission from the GaAs buffer layer at 1.513 eV shows a significantly shorter lifetime ($\tau \simeq 0.15$ ns) than the emission from the 2DHG ($\tau \simeq 0.4$ ns). This can be taken as direct evidence for the fact that spatially *indirect* transitions contribute to the 2DHG luminescence[37,38] as shown schematically in Fig. 1. For excitation at 3.07 eV (Fig. 7), spectra recorded directly after the exciting laser pulse ($t = 20$ ps) show a pronounced high-energy tail which indicates a nonthermalized carrier distribution. Here this effect is much more pronounced than for excitation at 1.73 eV, even though the excitation intensities are comparable, because of the smaller penetration depth and much larger excess energy of 3.07-eV photons. After thermalization of this initial hot carrier distribution ($t > 0.2$ ns) a FES develops in the PL spectrum. The FES decays with a time constant comparable to the decay time of the entire 2DHG emission spectrum of $\simeq 0.3$ ns. After thermalization of the photogenerated carriers the shape of the emission spectrum is essentially time independent, indicating that the recombination rate is independent of the emission energy. This contrasts with results reported for n-type modulation-doped heterojunctions and p-n-p double heterostructures where the PL decay time was found to vary with energy by several orders of magnitude.[37,38]

Figure 8 shows a sequence of temperature-dependent PL spectra from sample no. 4 all excited at 3.00 eV. For sample temperatures ≥ 25 K the FES is, as expected,[23,25,30,32] no longer resolved. Increasing the temperature further a third peak develops at the high-energy side of the 1.496-eV emission band. This new peak becomes the dominant feature in the spectrum for temperatures ≥ 75 K. Simultaneously the first two luminescence bands shift to lower energies which reflects the temperature dependence of the GaAs band-gap energy. This third peak arises from recombination involving higher-lying subbands which get thermally populated [for a justification of this assignment see the results of self-consistent subband calculations presented in Sec. IV, Figs. 10 and 11(a)]. Holes occupying such higher-lying subbands have in general more extended wave functions (see Sec. IV) than those in the lower subbands, resulting in an enhanced wave-function overlap with the photogenerated electrons. This enhanced overlap explains the comparatively strong emission intensity of this third peak even though relatively few holes are thermally excited into these higher-lying subbands.

To discriminate between emission from light- and heavy-hole subbands PL spectra were excited with circularly polarized light, and the degree of circular polarization of the emitted light was analyzed. Typical low-temperature difference spectra $I^+ - I^-$ for samples nos. 2–4 are shown in Fig. 9. Here I^+ and I^- denote the intensities of right and left circularly polarized emitted light, respectively. In Fig. 10 are shown spectra for sample no. 4 which were recorded with the sample held at 50 K to populate also higher-lying subbands (see the above discussion). The spectrum of the total intensity $I^+ + I^-$ mirrors the corresponding spectrum of unpolarized light (see Figs. 4, 5, and 8). In the difference spectrum $I^+ - I^-$, in contrast, transitions involving light-hole levels contribute subtractively.[39] In the low-temperature spectra from samples nos. 2 and 3 in Fig. 9, the negative contribution to the difference spectra from the light-hole level is clearly observed. From a comparison with the spectra of unpolarized light in Fig. 4 it can be seen that

the luminescence peak observed from samples nos. 2 and 3 is composed of overlapping transitions from heavy- *and* light-hole subbands. For sample no. 4 the lowest-energy emission band appears at a reduced relative intensity in the difference spectrum (Figs. 9 and 10) to that in the total intensity spectrum (Figs. 5 and 10), which again indicates the contribution of heavy- and light-hole transitions to this band. The emission from the light-hole band occurs at energies between the lowest heavy-hole transition centered at 1.45 eV and a second heavy-hole transition at 1.49 eV. For the 50-K spectra of sample no. 4 shown in Fig. 10, the $I^+ - I^-$ spectrum shows differences in the relative peak intensities as well as in the position of the peak with the highest energy, which occurs at a slightly lower energy in the difference spectrum $I^+ - I^-$ than in the total intensity spectrum $I^+ + I^-$. This indicates that the high-energy peak is a superposition of transitions from a heavy-hole and a light-hole subband, which contributes to the difference spectrum subtractively. The light-hole transition is at a somewhat higher energy than the heavy-hole one. An assignment to transitions from specific hole subbands will be given for samples nos. 3 and 4, based on results of self-consistent subband calculations, in Sec. IV.

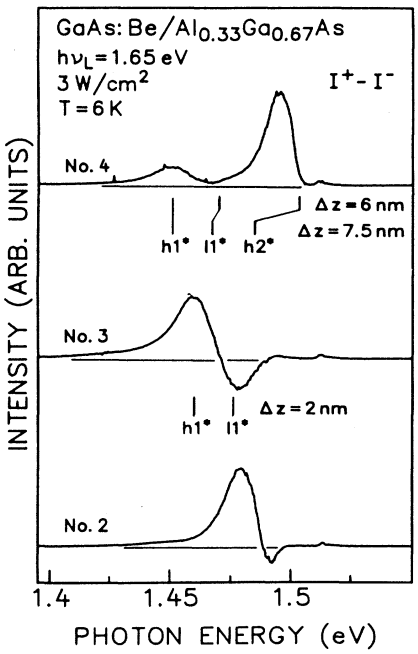

FIG. 9. Low-temperature (6 K) photoluminescence spectra of samples nos. 2–4 excited with right-hand circularly polarized light. The difference spectra $I^+ - I^-$ between right- and left-hand circularly polarized emission are displayed. Emission from a heavy-hole band results in a positive signal, that from a light-hole band in a negative signal. Subband energies, calculated for different dopant spreads Δz, are marked for samples nos. 3 and 4. The position of the first heavy-hole level hh1 is fixed at the peak of the lowest-energy band. Asterisks (*) indicate that the absolute energetic positions are not given but rather an indication of the expected peak positions.

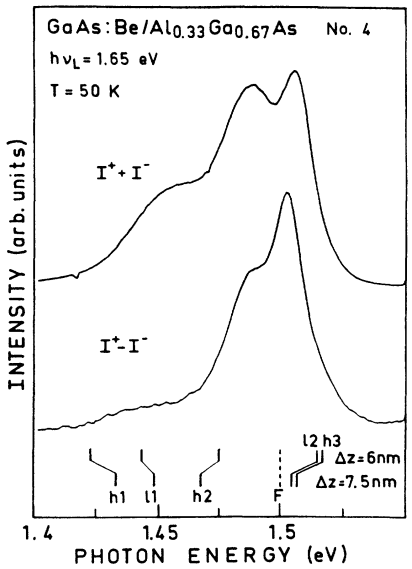

FIG. 10. 50-K luminescence spectra of sample no. 4 excited with right-hand circularly polarized light. The spectrum of the total intensity $I^+ + I^-$ and the difference spectrum between right- and left-hand circularly polarized emission $I^+ - I^-$ are displayed. Subband energies, calculated for 3×10^{13} cm^{-2} Be density and different dopant spreads Δz, are marked at the bottom of the figure (see Sec. IV).

IV. SELF-CONSISTENT SUBBAND CALCULATIONS

A. Valence-band structure

To determine the carrier confinement energies of a space-charge-induced potential well requires, within the Hartree approximation, a self-consistent solution of the Poisson and Schrödinger equations. In two-dimensional systems, coupling between heavy and light holes results in complicated valence-band structures with strongly nonparabolic bands, dispersions sometimes displaying electronlike masses.[40–45] Further to this, the forms of the hole subband wave functions vary with in-plane wave vector $k_\parallel$ due to the mixing between the bands.[42,46] So to determine the hole density distribution, it is necessary to calculate the valence-band structure and then explicitly sum the probability densities over states up to the Fermi level. This gives us in addition the Fermi energy, which can then be compared with the position of the Fermi-edge singularity in luminescence measurements (Sec. III). We calculate the valence-band structure within the multiband envelope-function approximation, from the Luttinger-Kohn Hamiltonian,[47] which describes the dispersions of, and interactions between, the heavy, light, and spin-orbit split-off bands up to order k^2. Details of the band-structure calculations are given in the Appendix.

For the structures considered here, inclusion of the split-off band was found to have very little effect upon the valence-band structure in the energy range of interest and so, for computational expediency, the split-off band was

neglected in the calculations presented below. The valence bands at large $k_{\|}$ are very anisotropic and a thorough calculation would involve calculating the band dispersions in all k directions, in order to determine the position of the Fermi level and distribution of holes throughout the subbands. However, again for computational expediency, the axial approximation was taken in which an average over the in-plane directions is made.[41]

We consider the structures to be symmetric with respect to the doping spike, the reasons for doing so to be discussed in Sec. IV B. For a given dopant concentration 100% ionization of acceptors is assumed, with 8×10^{10} cm^{-2} of the holes going towards both the surface and substrate, the remaining holes creating the quasi-two-dimensional hole gas of interest. This transfer of holes to traps in the buffer layer and substrate creates the necessary band bending to give Fermi-level pinning mid-bandgap at the semi-insulating substrate. We have taken the spread of dopants Δz as a variable parameter, keeping the sheet dopant concentration fixed and varying the volume concentration. The dopant atoms are taken to be homogeneously distributed over Δz. In Figs. 11(a) and 11(b) we illustrate the self-consistent potential profiles for sheet dopant concentrations of (a) 3×10^{13} cm^{-2} with a dopant spread of 6 nm; (b) 8×10^{12} cm^{-2} and 2 nm spread, the dopant spreads consistent with SIMS data which can only give an upper limit of the actual spike width (see Sec. II). Also shown are the zone-center ($k_{\|}=0$) energy levels and probability densities $|\psi|^2$ [where $\psi(z)$ are the envelope wave functions]. What is immediately apparent is the very strong localization of the hole density around the dopant spike, with a confinement length of only ~10 nm. This is to be compared with a greater spread of electrons in similar high-density n-type structures.[2,3,10] The intercepts of the subband energies of the unoccupied levels with the confining potential give an indication of the onset of the decay of the wave functions. As can be seen from Fig. 11, the wave-function spread of these levels is significantly larger than that of the occupied levels, with a spread of ~22 nm for the higher-density structure (a).

Figures 12(a) and 12(b) show the valence-band structures for these two systems, taken in the axial approximation. The strongly nonparabolic nature and anticrossings between the bands are instantly apparent. The labeling of the bands as the different quantized (i) heavy-hole (hh$i$) or light-hole (lh$i$) levels is only relevant at $k_{\|}=0$, as away from the zone center the states become strong mixtures of the different angular momentum states.[42] We illustrate in Figs. 13(a) and 13(b) the variation with dopant spread Δz of the hole confinement energies (at $k_{\|}=0$) and the Fermi energy for the two structures. Energies are with respect to the valence-band maximum at the center of the dopant spike. At a dopant spread Δz of 8 nm for the high-density structure there is a kink in the curves of Fig. 13(a) indicating occupation of a new subband. Although the Fermi level has still not crossed the lh2 level at $k_{\|}=0$, hole occupation of this band commences at this point at nonzero $k_{\|}$. From Fig. 12(a) we can see that the lh2 band initially has an electronlike mass and the band dispersion has a minimum at nonzero $k_{\|}$ where a pocket of holes initially forms. This emphasizes the need to consider the full band structure when considering self-consistent solutions of quasi-2D hole gases.

For the lower-density structure there is very little variation with dopant spread of the confinement energies [Fig. 13(b)], with just the potential maximum increasing in energy with decreasing spread as the "V"-shaped potential profile becomes more pronounced. For the whole range of dopant spread considered, the wave-function extent of the hole states is greater than that of the dopant spread, thus making the energy levels fairly insensitive to the form of the potential around the dopants. On the other hand, for the high-density structure [Fig. 13(a)], for large dopant spreads $\Delta z \geq 7$ nm the extent of the hole density matches very closely that of the dopants. Thus we progress from a parabolic to a square potential profile

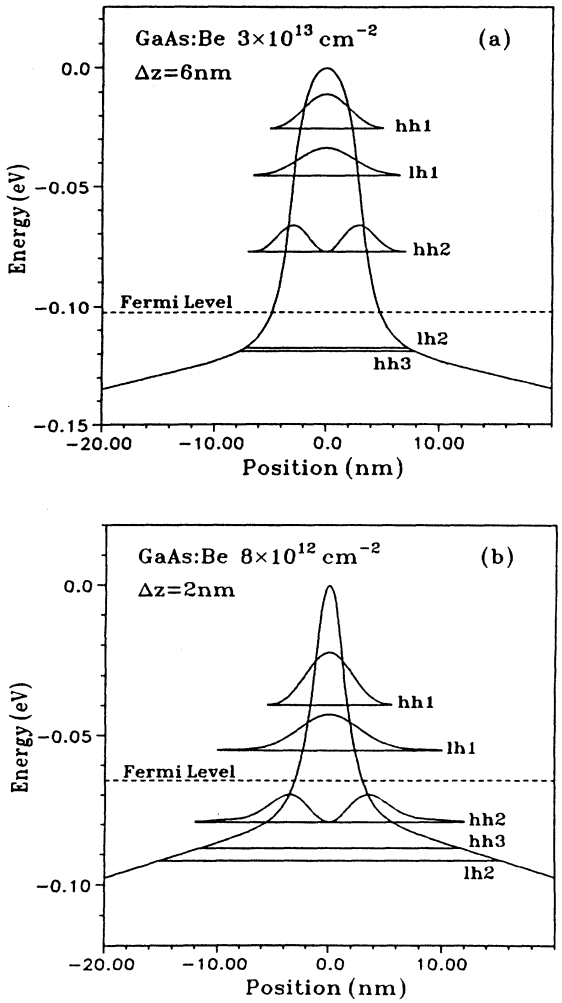

FIG. 11. Self-consistent potential profiles for the quasi-two-dimensional hole gas at a Be δ-doped layer in GaAs. (a) 3×10^{13} cm^{-2} Be density with 6-nm dopant spread. (b) 8×10^{12} cm^{-2} Be with 2-nm dopant spread. Subband energies and probability densities $|\psi(z)|^2$ at $k_{\|}=0$ are also shown. "hh" and "lh" denote heavy hole and light hole, respectively. Note the vertical scales for (a) and (b) are different.

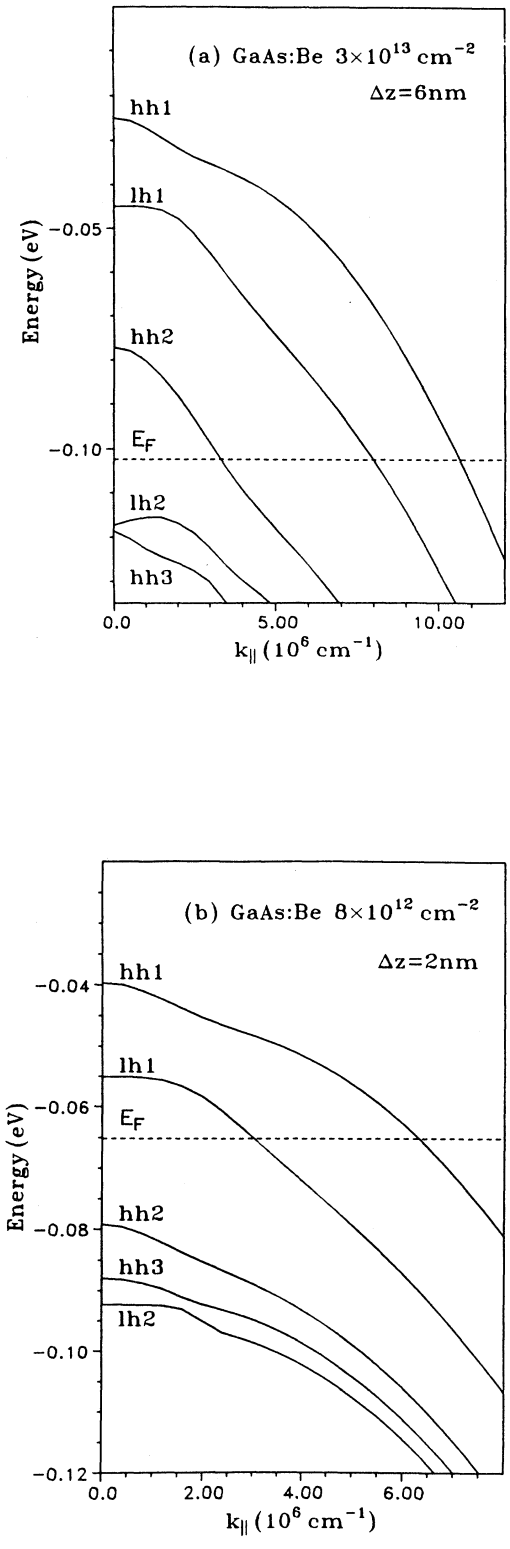

FIG. 12. Valence-band structures for (a) 3×10^{13} cm^{-2} Be with 6-nm dopant spread, (b) 8×10^{12} cm^{-12} Be with 2-nm dopant spread. "E_F" denotes the Fermi level and "hh" and "lh," the angular momentum character (whether heavy hole or light hole, respectively) at the zone center. Note the scales for (a) and (b) are different.

as the dopant spread increases and the volume concentration correspondingly decreases and so comes into line with that of the hole density. This gives rise to a much stronger variation of the confinement energies as well as the subband spacings with dopant spread, as can be readily seen from Fig. 13(a), thus enabling a comparison of the subband energies with luminescence measurements as a characterization of the dopant spread.

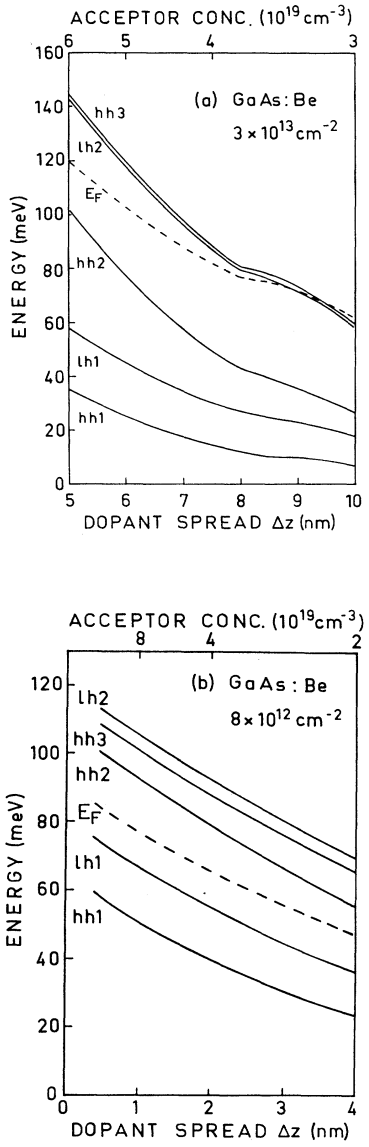

FIG. 13. Variation of hole subband energies, at $k_{\|}=0$, with respect to the valence-band maximum at the center of the dopant spike, as a function of dopant spread Δz. (a) 3×10^{13} cm^{-2} Be density, (b) 8×10^{12} cm^{-2} Be. For convenience the negatives of the energies are in fact plotted, i.e., they are given as positive. For comparison the horizontal scale at the top gives the volume dopant concentration resulting from the given two-dimensional dopant concentration and the actual dopant spread Δz. Note the scales for (a) and (b) are different.

B. Comparison with luminescence data

Using the Fermi energy as a reference point, given by the Fermi-edge singularity, we have compared the results of our self-consistent calculations of the valence-subband structure with the photoluminescence measurements. It should be noted that it is difficult to unambiguously determine the interband transition energies of a 2D plasma from the luminescence spectrum.[48] Thus we do not attempt here to make a thorough quantitative comparison between theory and experiment, but rather a more qualitative understanding of the subband structure of the systems under investigation.

The zone-center energies for a 3×10^{13} cm^{-2} acceptor concentration are shown in Figs. 5 and 10, with respect to the Fermi level given by the Fermi-edge singularity. In the low-temperature measurements of Fig. 5 the Fermi-edge singularity is clearly resolved and we take the high-energy side of the peak to indicate the Fermi level. For the high-temperature measurements shown in Fig. 10 we have fixed the Fermi level, which is not well defined in the experimental spectrum, at 1.5 eV. In Fig. 9 the energies are given relative to the first quantized heavy-hole level hh1 which is fixed at the low-energy peak. The energy ranges are given for a dopant spread between 6 and 7.5 nm corresponding, respectively, to a volume concentration between 5.0 and 4.0×10^{19} cm^{-3}.

If we focus on the circular-polarized luminescence results of Figs. 9 and 10, we can see that the ordering and spacing of the levels is correctly predicted below the Fermi level. It transpires that the low-energy peak of the photoluminescence of sample no. 4, given in Fig. 5 and by the sum spectrum $I^+ + I^-$ in Fig. 10, is a superposition of the first quantized heavy-hole (hh1) and light-hole (lh1) states. The second peak is due to the second heavy-hole level (hh2). Remembering that in the difference spectrum $I^+ - I^-$ (Figs. 9 and 10) the light-hole contribution is a negative signal, we can see that the energy levels are well reproduced by the calculations. For the states above the Fermi level, from which radiative recombination occurs upon thermal population, agreement is not so good. The prediction from calculations that the hh3 and lh2 levels should be close to one another is confirmed by a comparison of the sum and difference circularly polarized spectra of Fig. 10. However, it appears that their ordering is reversed and they are further in energy from the occupied levels than predicted. This is most probably due to changes in the self-consistent potential upon the thermal occupation of these bands. These changes in the potential will be less significant closer to the doped layer and so the lower occupied levels will not be affected. The fact that the higher quantized levels are sensitive to the electric field away from the spike, for which a rather arbitrary value was taken (see Sec. IV A) due to the uncertainties in substrate and surface depletion, may also be a cause of this discrepancy. In addition, due to the proximity to one another of these bands, there is a large amount of mixing at even small $k_{\parallel}$, this leading to the electronlike mass of the lh2 band. Thus the angular momentum character of the bands quickly changes away from the zone center, giving rise to some possible ambiguity in the circularly polarized results. From the general good agreement between experiment and theory, we can conclude for this structure (sample no. 4) a dopant spread of ~6.7 nm (in qualitative agreement with SIMS), with a Be volume concentration of $\sim4.5\times10^{19}$ cm^{-3}.

We compare in Figs. 3 and 9 the results of our calculations for an 8×10^{12} cm^{-2} acceptor concentration with the luminescence measurements of sample no. 3. We have taken a dopant spread of 2 nm, corresponding to a volume concentration of 4×10^{19} cm^{-3}. This is rather arbitrary due to the small variation in the subband spacings for this structure [Fig. 13(b)]. SIMS results indicate that there may be a slight spread of dopants (see Table I) and the general agreement between experiment and theory is good. In particular, from Fig. 9 it can be seen that the spacing between the hh1 and lh1 levels is well reproduced.

Approximations made in the calculations restrict a quantitative analysis. As stated earlier, neglecting the spin-orbit split-off band was found to affect the self-consistent potential and subband levels very little. Further simplifications made have been to neglect effects of the high hole density and high concentration of dopant atoms on the band structure. Although we can ignore band-gap renormalization[49,50] since we are only concerned here with subband spacings, second-order effects on the actual band dispersions could be significant.[50] However, the axial approximation made is perhaps a greater cause for error, especially for the determination of the Fermi level. In addition, at the high carrier densities and hence large wave vectors considered, the $\mathbf{k}\cdot\mathbf{p}$ method employed may no longer be a good approximation. To counter this, we note that the agreement with experiment for the energy levels with respect to the Fermi level is very good.

Let us now return to Fig. 11 and consider the potential profiles in greater detail. As stated earlier, we have assumed the potentials to be symmetric with just small electric fields outside the space-charge region, corresponding to a small transfer of only $\sim10^{11}$ cm^{-2} holes to remote traps on the surface and substrate sides. But the dopant spike is only 41 nm below the surface and so we should expect, in principle, a large electric field on the surface side due to Fermi-level pinning, with $\sim10^{12}$ cm^{-2} surface charge. But it is known that the pinning or unpinning of the Fermi level at the surface, and thus the strength of the surface electric field, is affected by light illumination.[51] It has been shown for n-type δ-doped GaAs:Si/$Al_xGa_{1-x}As$ double heterostructures with identical layer thicknesses that illumination with 1.65-eV photons at power densities ≥ 10 W/cm^2 results in essentially symmetric potential profiles.[52] It has been further shown by measurements of the electric-field-induced resonant Raman scattering of the GaAs LO phonon[53–55] that in the present sample structure for both n- and p-type doping the resulting electric field at the surface side of the δ-doped GaAs layer is strongly reduced by optical illumination.[52,56] Therefore we feel that it is not too unrealistic to assume an essentially symmetric potential profile for the above subband calculations. However, we would like to emphasize that, whether there is indeed surface Fermi-level pinning or not, the self-consistent poten-

tial and subband structure of the occupied hole bands determined in the present calculations are relatively unaffected by the position of the Fermi level at the surface because of the very localized nature of the hole confining potential.

Finally we consider the origin of the Fermi-edge singularity observed in the luminescence spectra (Figs. 3–5 and 7). Many of the reported observations of the Fermi-edge singularity in the photoluminescence of quasi-two-dimensional electron systems have been made possible by the localization of photocreated holes in a sufficiently flat valence band.[23–28,31,35] The singularity is due to multiple electron-hole scattering around the Fermi level, with electrons at $k=k_F$ and recombination to holes at $k\sim 0$; hole localization (hence spread in k space) and a low-dispersion hole band permit optical emission. For the quasi-two-dimensional hole systems under investigation here, emission now involves electrons near $k=0$. The electron effective mass is small and the electrons are unlikely to be localized. Hence the spread in k space of electron states will be very small and so, on these grounds, it should be unlikely to observe the Fermi-edge singularity. However, the valence-subband structures shown in Figs. 12(a) and 12(b) indicate a possible mechanism for the strong Fermi-edge enhancement observed in the emission spectra of sample no. 4. It has been observed that the presence of an unoccupied band close to the Fermi level can cause a large enhancement of the optical matrix elements, due to a hybridization between the Fermi-edge resonance and virtual excitons involving the unoccupied band.[29,33,34] This is analogous to an edge singularity occurring at $k\sim 0$ and so the need for localization of the minority carrier is relaxed. In these samples there does exist such a band: the lh2 level in sample no. 4 [Fig. 12(a)] and the hh2 level in sample no. 3 [Fig. 12(b)]. We conclude that these levels are most probably involved in the origin of the Fermi-edge enhancement. As further support for this argument we note that the lh2 level in sample no. 4 is closer in energy to the Fermi level than the hh2 level of no. 3. Thus it is expected that the Fermi-edge enhancement will be stronger for sample no. 4 than for no. 3 (Ref. 33) and this is indeed observed to be the case. However, further theoretical work is required, in particular to provide insight into why the enhancement is only observed for excitation by photon energies exceeding the $Al_xGa_{1-x}As$ barrier band-gap energy.

V. CONCLUSIONS

We have presented a detailed photoluminescence study of Be δ-doped GaAs layers. To compliment cw PL measurements, time-resolved experiments and measurements using circularly polarized light have also been performed. To enhance the 2DHG emission intensity $Al_xGa_{1-x}As/GaAs/Al_xGa_{1-x}As$ double heterostructures were prepared with the Be δ-doping spike placed in the center of the 60-nm-wide GaAs layer. Strong luminescence is observed from the 2DHG involving various subbands. In structures where the Fermi level lies close to unoccupied subbands a pronounced Fermi-edge singularity is observed in the PL spectrum. This Fermi-edge enhancement in emission intensity can be explained by a transfer of excitonic oscillator strength from unoccupied subbands to occupied states at the Fermi edge. The present observation of a FES in the emission spectrum of a 2DHG is facilitated by the *p*-type δ-doped double heterostructure used which enabled us to generate a dense 2DHG with free-hole concentrations exceeding 10^{13} cm^{-2}. Such hole concentrations might be difficult to achieve, for example, in *p*-type modulation-doped $Al_xGa_{1-x}As/GaAs$ heterostructures because of the comparatively small valence-band offset. To determine the hole confining potential and the valence-subband structure, self-consistent subband calculations have been performed. Taking into account the increasing spread of the dopant atoms with increasing dopant concentration, which is indicated independently by SIMS, the calculated subband spacings are in good agreement with those deduced from the PL experiments.

ACKNOWLEDGMENTS

We would like to thank P. Koidl and M. Ramsteiner for helpful discussion and H. S. Rupprecht for continuing support of the work at the Fraunhofer-Institut. D.R. wishes to thank U. Ekenberg for valuable help and discussions. Expert experimental assistance by F. Pohl and K. Schwarz is gratefully acknowledged. Part of the work at the Max-Planck-Institut was sponsored by the Bundesministerium für Forschung und Technologie (Bonn, Federal Republic of Germany).

APPENDIX

The band structure of the three highest (doubly degenerate) valence bands of zinc-blende semiconductors can be described by the Luttinger Hamiltonian.[47] This is a 6×6 matrix, the basis set for which comprises the four spin-$\frac{3}{2}$ (heavy hole $|\frac{3}{2},\pm\frac{3}{2}\rangle$, light-hole $|\frac{3}{2},\pm\frac{1}{2}\rangle$) and the two spin-$\frac{1}{2}$ (split off $|\frac{1}{2},\pm\frac{1}{2}\rangle$) zone-center states. Here we have used the $|J,\pm M_J\rangle$ notation for the angular momentum states at the Γ point. By a unitary transformation the 6×6 Hamiltonian can be block diagonalized to two 3×3 matrices,[45,57] effectively describing "spin-up" and "spin-down" states.

To calculate the valence-band structure of the quasi-two-dimensional hole system we employ the envelope-function approximation and replace, in the usual manner, the wave vector k_z in the confinement z direction by its associated momentum operator $-id/dz$. Thus we need to solve for the two Hamiltonians $H_\pm$ to give the subband dispersions and envelope wave functions:[42,45,58]

$$H_\pm=\begin{pmatrix} A_+ & C\mp iB & \sqrt{2}C\pm iB/\sqrt{2} \\ C\pm iB & A_- & F\mp i\sqrt{3/2}B \\ \sqrt{2}C\mp iB/\sqrt{2} & F\pm i\sqrt{3/2}B & D \end{pmatrix}, \tag{A1}$$

$$A_\pm=-\tfrac{1}{2}(\gamma_1\pm\gamma_2)k_\parallel^2+\tfrac{1}{2}(\gamma_1\mp 2\gamma_2)d^2/dz^2+V(z)\,, \tag{A2}$$

$$iB=\sqrt{3}\gamma_3 k_\parallel d/dz,\quad C=\sqrt{3/2}\gamma_c k_\parallel^2\,, \tag{A3}$$

$$D=-\Delta_0-\tfrac{1}{2}\gamma_1 k_\parallel^2+\tfrac{1}{2}\gamma_1 d^2/dz^2+V(z)\,. \tag{A4}$$

The matrix is with respect to a basis set of heavy, light, and spin-orbit split-off holes, respectively. Δ_0 is the split-off band gap. γ_1, γ_2, γ_3 are the Luttinger parameters and the parameter γ_c is a function of the crystallographic direction $k_\parallel$ and accounts for the anisotropy of the valance bands. Here we employ the axial approximation for the valence bands where $\gamma_c = \frac{1}{2}(\gamma_2 + \gamma_3)$.[41] $V(z)$ is the confining potential. Neglecting the split-off band reduces the Hamiltonian $H_\pm$ to 2×2 block matrices.

Eigenvalues and envelope wave functions are determined using a modified variational method.[58,59] This expands the wave functions in terms of a set of basis functions and so keeps the problem in terms of a matrix eigenvalue problem, each element of $H_\pm$ now becoming a block matrix with respect to the basis functions. For a symmetric potential, the "spin-up" and "spin-down" subbands are degenerate. However, it should be noted that the wave functions are not symmetric at nonzero $k_\parallel$, due to the lack of inversion symmetry of GaAs.[59] They are, however, antisymmetric to one another, leading to a symmetric probability density. A self-consistent solution between the band-structure calculations and the Poisson equation is obtained in the usual way,[60] with the proviso of the need for summing over occupied states explicitly, as outlined in Sec. IV.

---

*Present address: Cavendish Laboratory, Madingley Road, Cambridge CB3 0HE, U.K.

†Present addrress: Institut für Experimentalphysik, Johannes-Kepler-Universität, A-4040 Linz, Austria.

‡Present address: Paul-Drude-Institut für Festkörperelektronik, Hausvogteiplatz 5-7, O-1086 Berlin, Federal Republic of Germany.

[1]For a recent review see K. Ploog, M. Hauser, and A. Fischer, Appl. Phys. A **45**, 233 (1988); E. F. Schubert, J. Vac. Technol. A **8**, 2980 (1990).

[2]F. Koch and A. Zrenner, Mater. Sci. Eng. B **1**, 221 (1989), and references therein.

[3]A. Zrenner, F. Koch, and K. Ploog, in *Proceedings of the 14th International Symposium on GaAs and Related Compounds*, edited by A. Christou and H. S. Rupprecht, IOP Conf. Proc. No. 91 (Institute of Physics and Physical Society, London, 1988), p. 171.

[4]R. B. Beall, J. B. Clegg, and J. J. Harris, Semicond. Sci. Technol. **3**, 612 (1988).

[5]E. F. Schubert, J. B. Stark, B. Ullrich, and J. E. Cunningham, Appl. Phys. Lett. **52**, 1508 (1988).

[6]M. Santos, T. Sajoto, A. Zrenner, and M. Shayegan, Appl. Phys. Lett. **53**, 2504 (1988).

[7]A.-M. Lanzillotto, M. Santos, and M. Shayegan, Appl. Phys. Lett. **55**, 1445 (1989).

[8]J. Wagner, M. Ramsteiner, W. Stolz, M. Hauser, and K. Ploog, Appl. Phys. Lett. **55**, 978 (1989).

[9]E. F. Schubert, H. S. Luftman, R. F. Kopf, R. L. Headrick, and J. M. Kuo, Appl. Phys. Lett. **57**, 1799 (1990).

[10]A. Zrenner, F. Koch, R. L. Williams, R. A. Stradling, K. Ploog, and G. Weimann, Semicond. Sci. Technol. **3**, 1203 (1988).

[11]G. Abstreiter, R. Merin, and A. Pinczuk, IEEE J. Quantum Electron. **22**, 1771 (1986).

[12]J. Wagner, M. Ramsteiner, D. Richards, G. Fasol, and K. Ploog, Appl. Phys. Lett. **58**, 143 (1991).

[13]M. H. Degani, Phys. Rev. B **44**, 5580 (1991).

[14]S. J. Pearton, F. Ren, C. R. Abernathy, W. S. Hobson, S. N. G. Chu, and J. Kovalchick, Apply. Phys. Lett. **55**, 1342 (1989).

[15]E. F. Schubert, J. M. Kuo, R. F. Kopf, H. S. Luftman, L. C. Hopkins, and N. J. Sauer, J. Appl. Phys. **67**, 1969 (1990).

[16]O. Ourmazd, J. Cunningham, W. Jan, J. A. Rentschler, and W. Schröter, Appl. Phys. Lett. **56**, 854 (1990).

[17]J. Wagner, A. Ruiz, and K. Ploog, Phys. Rev. B **43**, 12 134 (1991).

[18]C. H. Perry, K. S. Lee, W. Zhou, J. M. Worlock, A. Zrenner, F. Koch, and K. Ploog, Surf. Sci. **196**, 677 (1988).

[19]J. C. M. Henning, Y. A. A. R. Kessener, P. M. Koenraad, M. R. Leys, W. van der Vleuten, J. H. Wolter, and A. M. Frens, Semicond. Sci. Technol. **6**, 1079 (1991).

[20]J. Wagner, A. Fischer, and K. Ploog, Phys. Rev. B **42**, 7280 (1990).

[21]J. Wagner, A. Fischer, and K. Ploog, Appl. Phys. Lett. **59**, 428 (1991).

[22]A. M. Gilinsky, K. S. Zhuravlev, D. I. Lubyshev, V. P. Migal, V. V. Preobrazhenskii, and B. R. Semiagin, Superlatt. Microstruct. **10**, 399 (1991).

[23]M. S. Skolnick, J. M. Rorison, K. J. Nash, D. J. Mowbray, P. R. Tapster, S. J. Bass, and A. D. Pitt, Phys. Rev. Lett. **58**, 2130 (1987).

[24]G. Livescu, D. A. B. Miller, D. S. Chemla, M. Ramaswamy, T. Y. Chang, N. Sauer, A. C. Gossard, and J. H. English, IEEE J. Quantum. Electron. **QE-24**, 1677 (1988).

[25]R. Cingolani, W. Stolz, and K. Ploog, Phys. Rev. B **40**, 2950 (1989).

[26]H. Kalt, K. Leo, R. Cingolani, and K. Ploog, Phys. Rev. B **40**, 12 017 (1989).

[27]Yong-Hang Zhang, De-Sheng Jiang, R. Cingolani, and K. Ploog, Appl. Phys. Lett. **56**, 2195 (1990).

[28]S. R. Andrews, A. S. Plaut, R. T. Harley, and T. M. Kerr, Phys. Rev. B **41**, 5040 (1990).

[29]W. Chen, M. Fritze, A. V. Nurmikko, D. Ackley, C. Colvard, and H. Lee, Phys. Rev. Lett. **64**, 2434 (1990); W. Chen, M. Fritze, A. V. Nurmikko, M. Hong, and L. L. Chang, Phys. Rev. B **43**, 14 738 (1991).

[30]M. S. Skolnick, D. M. Whittaker, P. E. Simmonds, T. A. Fisher, M. K. Saker, J. M. Rorison, R. S. Smith, P. B. Kirby, and C. R. H. White, Phys. Rev. B **43**, 7356 (1991).

[31]Z. H. Zhang, N. N. Ledentsov, and K. Ploog, Phys. Rev. B **44**, 1399 (1991).

[32]S. Schmitt-Rink, C. Ell, and H. Haug, Phys. Rev. B **33**, 1183 (1986).

[33]J. F. Mueller, Phys. Rev. B **42**, 11 189 (1990).

[34]P. Hawrylak, Phys. Rev. B **44**, 6262 (1991).

[35]I. E. Perakis and Y.-C. Chang, Phys. Rev. B **43**, 12 556 (1991).

[36]M. Cardona and G. Harbeke, J. Appl. Phys. **34**, 813 (1962); D. E. Aspnes, S. M. Kelso, R. A. Logan, and R. Bhat, *ibid.* **60**, 754 (1986).

[37]See, e.g., J. P. Bergman, Q. X. Zhao, P. O. Holtz, B. Monemar, M. Sundaram, J. L. Merz, and A. C. Gossard, Phys. Rev. B **43**, 4771 (1991).

[38]G. D. Gillard, D. J. Wolford, T. F. Kuech, and J. A. Bradley, Phys. Rev. B **43**, 14 251 (1991).
[39]See, e.g., *Optical Orientation,* edited by F. Meier and B. P. Zakhachenya (North-Holland, Amsterdam, 1984); M. Kunzer, G. Hendorfer, U. Kaufmann, and K. Köhler, Phys. Rev. B **45**, 11 151 (1992).
[40]M. Altarelli, U. Ekenberg, and A. Fasolino, Phys. Rev. B **32**, 5138 (1985).
[41]U. Ekenberg and M. Altarelli, Phys. Rev. B **32**, 3712 (1985).
[42]E. P. O'Reilly, Semicond. Sci. Technol. **4**, 121 (1989).
[43]R. Eppenga, M. F. H. Shuurmans, and S. Colak, Phys. Rev. B **36**, 1554 (1987).
[44]L. Eaves, R. K. Hayden, M. L. Leadbeater, D. K. Maude, E. C. Valadaras, M. Henini, F. W. Sheard, O. H. Hughes, J. C. Portal, and L. Cury, Surf. Sci. **263**, 199 (1992).
[45]A. M. Cohen and G. E. Marques, Phys. Rev. B **41**, 10 608 (1990).
[46]U. Ekenberg, Surf. Sci. **229**, 419 (1990).
[47]J. M. Luttinger and W. Kohn, Phys. Rev. **97**, 869 (1955); J. M. Luttinger, *ibid.* **102**, 1030 (1956).
[48]G. E. W. Bauer and T. Ando, Phys. Rev. B **34**, 1300 (1986).
[49]C. Delalande, G. Bastard, J. Organasi, J. A. Brum, H. W. Liu, M. Voos, G. Weimann, and W. Schlapp, Phys. Rev. Lett. **59**, 2690 (1987); G. E. W. Bauer, Surf. Sci. **229**, 374 (1990).
[50]B. E. Sernelius, Phys. Rev. B **33**, 8582 (1986); G. Borghs, K. Bhattacharyya, K. Deneffe, P. Van Mieghem, and R. Mertens, J. Appl. Phys. **66**, 4381 (1989), and references therein.
[51]E. Yablonovitch, B. J. Skromme, R. Bhat, J. P. Harbison, and J. J. Gmitter, Appl. Phys. Lett. **54**, 555 (1989).
[52]D. Richards, J. Wagner, A. Fischer, and K. Ploog, Appl. Phys. Lett. **61**, 2685 (1992).
[53]F. Schäffler and G. Abstreiter, Phys. Rev. B **34**, 4017 (1986).
[54]H. Shen, P. Parayanthai, F. H. Pollack, R. N. Sacks, and G. Hickman, Solid State Commun. **63**, 357 (1987).
[55]W. Kauschke, N. Mestres, and M. Cardona, Phys. Rev. B **36**, 7469 (1987).
[56]D. Richards, J. Wagner, K. Ploog, and A. Fischer, in *Photo-Induced Space Charge Effects in Semiconductors,* edited by D. D. Nolte, N. M. Haegel, and K. W. Goosen, MRS Symposia Proceedings No. 261 (Materials Research Society, Pittsburgh, 1992), p. 63.
[57]D. A. Broido and L. J. Sham, Phys. Rev. B **31**, 888 (1985).
[58]U. Ekenberg, Phys. Rev. B **38**, 12 664 (1988); U. Ekenberg, W. Batty, and E. P. O'Reilly, J. Phys. (Paris) Colloq. **48**, C5-553 (1987).
[59]M. Altarelli, Phys. Rev. B **28**, 842 (1983).
[60]T. Ando, A. Fowler, and F. Stern, Rev. Mod. Phys. **54**, 437 (1982).